Microwave quantum optics as a direct probe of the Overhauser field in a quantum dot circuit quantum electrodynamics device

Pei-Qing Jin,[1] Jan Jeske,[2,3] Andrew D. Greentree,[2,4] and Jared H. Cole[2,5,*]

[1]*Institute of Logistics Engineering, Shanghai Maritime University, Shanghai 201306, China*
[2]*Chemical and Quantum Physics, School of Science, RMIT University, Melbourne, Victoria 3001, Australia*
[3]*Fraunhofer Institute for Applied Solid State Physics IAF, Tullastrasse 72, 79108 Freiburg, Germany*
[4]*Australian Research Council Centre of Excellence for Nanoscale BioPhotonics, RMIT University, Melbourne, Victoria 3001, Australia*
[5]*Australian Research Council Centre of Excellence in Exciton Science, RMIT University, Melbourne, Victoria 3001, Australia*

(Received 1 October 2020; revised 6 December 2020; accepted 9 December 2020; published 7 January 2021)

We show theoretically that a quantum dot circuit quantum electrodynamics device can be used as a probe of the Overhauser field in quantum dots. By coupling a transmission line to the interdot tunneling gate, an electromagnetically induced transparency scheme can be established, whose Fano-type interference leads to a sharp curvature in the reflection spectrum around resonance. This sharp feature persists even in the presence of the fluctuating spin bath, rendering a high-resolution method to extract the bath's statistical information. For strong nuclear spin fields, the reflection spectrum exhibits an Autler-Townes splitting, where the peak locations indicate the strengths of the Overhauser field gradient.

DOI: 10.1103/PhysRevB.103.045301

I. INTRODUCTION

A singlet-triplet qubit encoded in two-electron states in a double quantum dot [1] has emerged as a promising candidate for quantum dot based quantum information processing systems [2–7]. For quantum dots in III-V-type semiconductors the electrons interact with a large number of nuclear spins ($\sim 10^5$) residing in the host lattice. These nuclear spins provide a fluctuating magnetic field (Overhauser field) with a statistical variance of a few milliteslas [8,9]. This leads to a nanosecond-timescale dephasing time T_2^* for the electron spins [10,11]. Both electrical and optical methods have been employed to mitigate this effect [12–14]. Alternatively, the spin bath can also assist in quantum information processing, e.g., as a key ingredient in the universal control of a singlet-triplet qubit [5] or as a long-lived quantum memory [15]. Both of these aspects make it crucial to understand the Overhauser field and the nuclear spin bath that generates it.

For the singlet-triplet qubit in a double quantum dot, the Overhauser fields are usually different between the two dots due to, e.g., their geometric asymmetry. This leads to an Overhauser field gradient (OFG). So far, measurements of the OFG are based on a spin-to-charge conversion (e.g., in Refs. [4,13,16]). The whole procedure involves several steps, and a cyclic sequence of gate pulses is employed. After initialization, the system is moved to an operating point where the qubit experiences free precession under the OFG, and then the system is brought back to its initial state where its return probability reflects the OFG. The statistical variance of the OFG is then extracted from the Gaussian-like decay of the return probability.

Circuit quantum electrodynamics (CQED) devices provide a bridge from solid-state qubits to the photonic world. By coupling qubits to a superconducting transmission line [17,18], fascinating quantum optic phenomena such as single-qubit lasing [19,20] and cooling [21] and single-photon generation [22] and detection [23,24] have been achieved. Our interest here is in electromagnetically induced transparency (EIT) [25], which provides efficient control over optical responses of atomic systems and thus gives rise to numerous applications, including precision measurement [26], quantum optical memories [27], and coherent electron transfer [28], and was also demonstrated in CQED systems [29,30]. Stimulated by success with CQED with superconducting qubits, theoretical proposals towards quantum dot based CQED devices were put forward [31–36]. Recent fast experimental progress includes atom-photon coupling in these hybrid systems [37,38], characterization of photon emissions [39,40], and construction of a quantum dot maser [41–45]. There has also been considerable interest in the interaction between quantum dot based CQED and phonons [39,41,46–49].

Here we propose an EIT-based method to detect the nuclear spin field in a double quantum dot via a CQED architecture, as shown in Fig. 1. The OFG breaks the spin conservation and mixes the singlet-triplet qubit states. When driving a probe field along the transmission line coupled to the interdot tunneling gate, the system can achieve EIT, where due to a Fano-type interference its reflection spectrum exhibits a double-peak structure with a sharp dip around resonance. The fluctuating nuclear spin bath imprints its statistical information on the spectrum whose sharp feature provides a high-resolution detection mechanism.

II. MODEL AND APPROACH

We consider a double quantum dot with two electrons. The detection mechanism involves two singlet-triplet states, $|1,1\rangle_S$ and $|1,1\rangle_{T_0}$, in the $m_s = 0$ subspace, as well as a

*jared.cole@rmit.edu.au

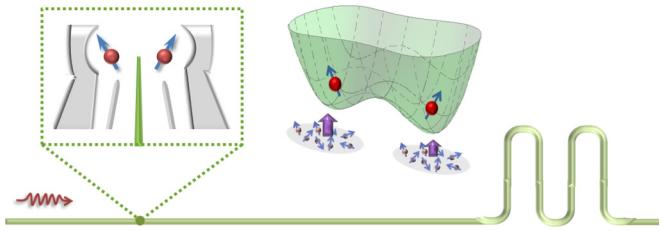

FIG. 1. Schematic of a quantum dot CQED device. A transmission line is coupled to the interdot tunneling gate of a double quantum dot system via a finger-shaped electrode extended from the transmission line. The quantum dots contain two electrons, both of which experience effective magnetic fields provided by the local nuclear spins.

singlet with two electrons occupying the right dot, $|0,2\rangle_S$. We assume the system operates in a parameter regime with negligible interdot tunneling where the nuclear spins exert a relatively large influence on the qubit [4,13]. The two qubit states are then degenerate and, by tuning gate voltages, can possess higher energy than state $|0,2\rangle_S$, as shown in Fig. 2(a).

The energy difference between the two singlet states, $|1,1\rangle_S$ and $|0,2\rangle_S$, denoted as ω_0 (throughout the paper we set $\hbar = 1$), depends on the dot detuning and on-site Coulomb interaction [3]. The singlet-triplet qubit states are coupled via the OFG (with strength Δh). Furthermore, we assume a transmission line is coupled to the interdot tunneling gate [35]. A probe field with frequency ω_p propagating through the transmission line then addresses the two singlets, $|1,1\rangle_S$ and $|0,2\rangle_S$, with Rabi frequency Ω_p. Then the Hamiltonian in the space spanned by $\{|0,2\rangle_S, |1,1\rangle_S, |1,1\rangle_{T_0}\}$ is given by

$$H_0 = \begin{pmatrix} 0 & \Omega_p \cos(\omega_p t) & 0 \\ \Omega_p \cos(\omega_p t) & \omega_0 & \Delta h \\ 0 & \Delta h & \omega_0 \end{pmatrix}. \quad (1)$$

This Hamiltonian indicates that, compared to a conventional situation [25], the quantum dot CQED system actually

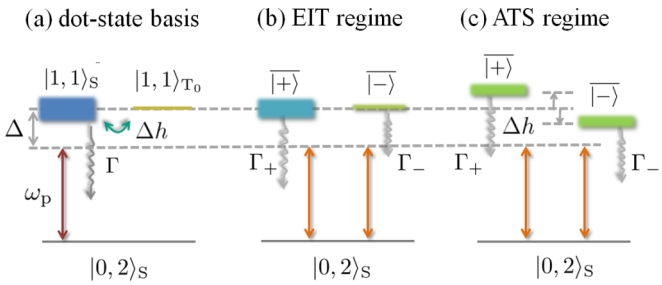

FIG. 2. (a) Relevant energy levels in a dot-state basis. The probe field with frequency ω_p addresses the transition between the two singlets, where a frequency detuning Δ is allowed. An OFG with magnitude Δh mixes the two qubit states. Charge noise renders a dominant decay channel from state $|1,1\rangle_S$ to $|0,2\rangle_S$ with rate Γ. Dressed-state picture for (b) EIT and (c) ATS regimes. The OFG couples the single-triplet qubit states, leading to two nuclear-spin-mediated states, $|\overline{\pm}\rangle$. The nuclear-spin-mediated states have the same energy but distinctive widths in the EIT regime (weak Δh), while they develop different frequencies separated by $2\Delta h$ but the same width $\Gamma_\pm = \Gamma/2$ in the ATS regime (strong Δh).

constitutes an (inverted) Λ configuration (a V configuration) where an EIT scheme can be established due to the spin selection rules preventing coupling between the singlet and triplet states. Here the OFG effectively plays the role of a dc coupling field, which is resonant with the corresponding electronic transition.

We analyze the dynamics of the system in a master-equation formalism with dissipation described by Lindblad operators [50],

$$\dot{\varrho} = -i[H_{RF}, \varrho] + \frac{\Gamma}{2}(2\sigma_- \varrho \sigma_+ - \varrho \sigma_+\sigma_- - \sigma_+\sigma_- \varrho), \quad (2)$$

where H_{RF} denotes an effective Hamiltonian in a rotating frame transformed under a unitary matrix $U_{RF} = \exp\{(-it)\mathrm{diag}(0, \Delta, \Delta)\}$ with detuning $\Delta = \omega_0 - \omega_p$, as well as the usual rotating wave approximation [51], ϱ represents the reduced density matrix for the dot system, and $\sigma_- \equiv |0,2\rangle_{SS}\langle 1,1|$. We focus on a dominant relaxation process from $|1,1\rangle_S$ to $|0,2\rangle_S$ caused by charge noise. The energy splitting between the qubit states and state $|0,2\rangle_S$ is resonant with the microwave drive and is therefore large compared to typical operating temperatures, which means we can ignore excitation processes and focus simply on the relaxation. The pure dephasing between states $|1,1\rangle_S$ and $|0,2\rangle_S$ can be included; however, this rate merely adds to the relaxation rate [25] without significantly changing the results. For the double quantum dot, a dephasing rate of a few hundred megahertz is typical [52], which is the same order as our assumed relaxation rate of $\Gamma/2\pi = 400$ MHz. Note that the relaxation from $|1,1\rangle_S$ to $|1,1\rangle_{T_0}$ is strongly suppressed due to spin conservation. This helps to protect the resulting EIT window, which would otherwise be deteriorated by such additional dissipation.

III. EIT SCHEME

Equation (1) suggests from the level-structure perspective that an EIT scheme can be established in the coupled system. Another prerequisite condition relies on the relative strength between the OFG and the electronic decay rate. It essentially determines whether the system is in an EIT or Autler-Townes-splitting (ATS) regime. Although the fundamentals of both EIT and ATS derive from the same interactions [25,53,54], it is nevertheless useful to distinguish between these two limits, where there is a smooth transition from EIT-like to ATS-like with increasing coupling [55]. In keeping with the recent literature we define the EIT regime as being where interference effects lead to subnatural linewidth features, and the ATS regime is where interference effects are not important for understanding the system properties. For illustration we adopt a dressed-state picture which was developed in the study of Fano-type interference in an EIT scheme [25,56]. In this picture, the EIT phenomenon results from the destructive interference between two scattering processes through two dressed states. In our case the OFG plays the role of a dc coupling field; we refer to these dressed states as "nuclear-spin-mediated" states. These states, $|\overline{\pm}\rangle$, are eigenstates of a non-Hermitian effective Hamiltonian including the electronic decay rate in the subspace of $\{|1,1\rangle_S, |1,1\rangle_{T_0}\}$, whose eigenvalues are $\Delta_\pm =$

$-(\pm\sqrt{16\,\Delta h^2-\Gamma^2}+i\Gamma)/4$. For weak OFG ($\Delta h/\Gamma \ll 1$), the nuclear-spin-mediated states are approximately the bare qubit states modified by a small hybridization, namely, $|\pm\rangle \simeq |1,1\rangle_{S/T_0} \pm \alpha|1,1\rangle_{T_0/S}$, with $\alpha = -2\Delta h/(i\Gamma)$. In this case, as shown in Fig. 2(b), the nuclear-spin-mediated states have the same frequency $\mathrm{Re}[\Delta_\pm] \simeq 0$ but distinct widths: one is close to the natural width of $|1,1\rangle_S$, namely, $\Gamma_+ = -\mathrm{Im}[\Delta_+] \simeq \Gamma/2 - 2\Delta h^2/\Gamma$; the other is much narrower, $\Gamma_- = -\mathrm{Im}[\Delta_-] \simeq 2\Delta h^2/\Gamma$. Then the scattering processes through either of these nuclear-spin-mediated states interfere destructively with each other, leading to a cancellation in the spectrum at resonance. This interference was identified as Fano-type interference [56]. For strong OFG compared to the decay rate, the nuclear-spin-mediated states are energetically shifted by $\pm\Delta h$, each with width $\Gamma/2$, as shown in Fig. 2(c). The scattering processes can then be viewed as two separate channels, resulting in two Lorentzian line shapes. This spectral structure is then an ATS, which in our case is a nuclear-spin-field-induced Stark effect.

IV. REFLECTION SPECTRUM

We use the reflection spectrum as a monitor of the OFG. Following a procedure similar to that in Ref. [29], we find the reflection coefficient $r = r_0(-i\Gamma/\Omega_p)_S\langle 1,1|\varrho|0,2\rangle_S$, where r_0 denotes a bare reflection coefficient with vanishing OFG. We then introduce $\mathcal{R} = |r/r_0|^2$ to characterize the renormalized strength of the reflection coefficient. By seeking the steady-state solution of Eq. (2), we obtain

$$\mathcal{R} = \frac{\Delta^2(\Gamma/2)^2}{(\Delta^2-\Delta h^2)^2+\Delta^2(\Gamma/2)^2}. \tag{3}$$

Figures 3(a) and 3(b) show the reflection spectrum as a function of detuning for different values of OFG. There are a few features of the spectrum which will be employed in our detection strategy. First, the spectrum exhibits a double-peak structure with maxima at $\Delta_{max} = \pm\Delta h$. Hence, the strength of the OFG can be extracted from the peak positions. Second, a sharp dip appears at the resonance $\Delta = 0$ for small OFG [blue line in Fig. 3(b)]. It is due to the Fano-type interference in the EIT regime. We approximate its detuning dependence as $|\partial\mathcal{R}/\partial\Delta| \simeq [\Gamma^2/(2\Delta h^4)]\Delta$, which clearly indicates increasing sensitivity for weak OFG. This sharp curvature can then serve as a promising basis for a high-resolution detection scheme. In addition, as the OFG grows, the spectral peaks move farther apart, as shown in Fig. 3(a). For strong OFG, either peak develops into a Lorentzian line shape with width $\Gamma/2$ [green line in Fig. 3(b)]. In this case the system is in an ATS regime, where the spectrum becomes rather flat around resonance (i.e., $\Delta \approx 0$).

Fluctuations in the OFG modify the reflection spectrum. So far we have treated the nuclear spin field as a static field, which due to its slow dynamics is valid for a single run of experiment. During the data collection, however, the Overhauser field fluctuates, leading to various magnitudes of the OFG for each independent experiment, the distribution of which takes a Gaussian form, $P(\Delta h) = (\sqrt{2\pi}\sigma)^{-1}\exp[-(\Delta h - h_0)^2/(2\sigma^2)]$ [9,10]. Its mean value h_0 depends on the polarization of the nuclear spins, which is typically a few milliteslas for an unpolarized nuclear spin bath [4], and can reach hundreds of milliteslas via external polarization mechanism [13]. The statistical variance σ can be several tenths of a μeV. The final result of the reflection is then based on an ensemble average over different nuclear spin configurations, given by

$$\langle\mathcal{R}\rangle_{nucl} = \frac{\sqrt{\pi}\,\Delta\Gamma}{4\sqrt{2}\,\sigma}\mathrm{Re}(Z_p^{-1}\{e^{-X_-^2}[1+\mathrm{Erf}(iX_-)] + e^{-X_+^2}[1-\mathrm{Erf}(iX_+)]\}), \tag{4}$$

where Erf(x) is the error function, $Z_p = \sqrt{\Delta}\sqrt{\Delta + i(\Gamma/2)}$, and $X_\pm = (\mp Z_p - h_0)/(\sqrt{2}\,\sigma)$. As shown in Figs. 4(a) and 4(b), the variance σ has a broadening effect on the spectral peaks. As σ grows, contributions to the averaged reflection spectrum come from a wider range of OFG. In Ref. [57] the effect of inhomogeneous broadening from frequency detuning on EIT phenomenon was studied. In contrast here the

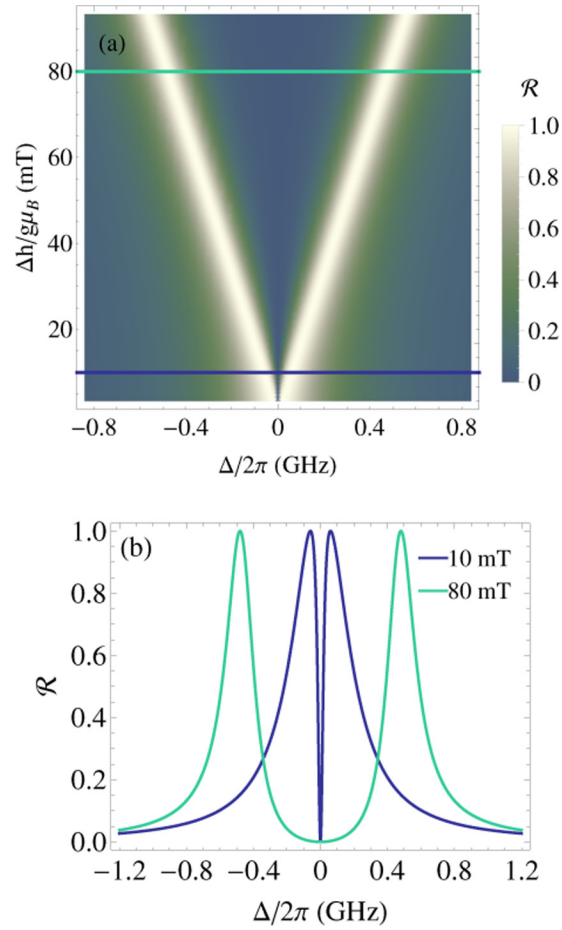

FIG. 3. (a) Density plot of reflection $\mathcal{R}$ as a function of both detuning and OFG. The spectrum exhibits a double-peak structure. As Δh increases, the spectral peaks move far apart, and the system develops from an EIT regime to an ATS regime. (b) Reflection as a function of detuning. For weak OFG with $\Delta h/(g\mu_B) = 10$ mT (blue line), the spectrum exhibits a sharp dip around the resonance $\Delta = 0$ due to Fano-type interference. For strong OFG with $\Delta h/(g\mu_B) = 80$ mT (green line), the peaks are well separated, and the spectrum becomes rather flat at the resonance.

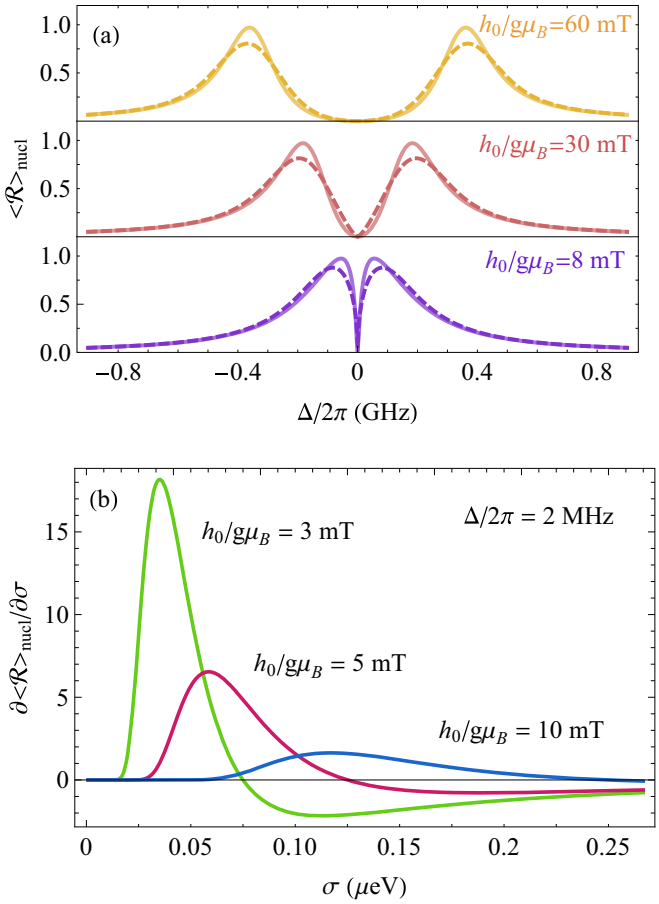

FIG. 4. (a) Ensemble-averaged reflection $\langle\mathcal{R}\rangle_{\rm nucl}$ as a function of detuning with OFG variance $\sigma = 75$ neV (solid lines) and $\sigma = 250$ neV (dashed lines). The spectral peaks get broadened by increasing variance. For small mean value $h_0/(g\mu_{\rm B}) = 10$ mT the sharp feature around the resonance persists even in the presence of variance. As the mean value increases, the spectrum starts to develop a flat profile at the resonance. Throughout the paper we choose $\Gamma/2\pi = 400$ MHz and consider GaAs quantum dots with $|g| = 0.44$. (b) Reflection sensitivity to statistical variance σ for different mean values h_0 at detuning $\Delta/2\pi = 2$ MHz. This sensitivity reduces with increasing mean value, where the spectrum becomes rather flat around the resonance.

broadening effect arises from the fluctuating strength of the coupling field, namely, the OFG.

V. DETECTION MECHANISM

A striking feature of the ensemble-averaged reflection is that the sharp curvature around the resonance in the EIT regime still persists in the presence of the variance, as shown in Fig. 4(a). We then adopt it as a sensitive measure to extract the variance σ. We expand $\langle\mathcal{R}\rangle_{\rm nucl}$ around the resonance, which can be approximated as $\langle\mathcal{R}\rangle^{(\rm L)}_{\rm nucl} = \sqrt{\pi\Gamma|\Delta|}/(2\sqrt{2}\sigma)\exp[-h_0^2/(2\sigma^2)]$. Its sensitivity on the variance is

$$\frac{\partial\langle\mathcal{R}\rangle^{(\rm L)}_{\rm nucl}}{\partial\sigma} = \left(\frac{\sqrt{\pi\Gamma|\Delta|}}{2\sqrt{2}}\right)\left(\frac{h_0^2-\sigma^2}{\sigma^4}\right)\exp\left(-\frac{h_0^2}{2\sigma^2}\right). \quad (5)$$

As shown in Fig. 4(b), the sensitivity reaches its maximum around $\sigma \simeq h_0/2$. For small variance $\sigma \ll h_0$, the broadening effect of the fluctuating OFG is weak, and the spectrum slope close to the resonance is still very sensitive to the variance, rendering a high detection resolution. However, as the mean value h_0 grows, the sensitivity decreases. This is because the system in this parameter regime falls into the ATS scheme, where the double peaks are well separated and the spectrum is rather flat around resonance. In this situation, the above detection mechanism is not available any more. Instead, one can return to the peak structure. Around each peak, the spectrum can be approximated as a Lorentzian profile. For weak variance, its ensemble-averaged result still locates around $\pm h_0$, with a peak value of $1 - 4\sigma^2$. The strategy is then to extract the variance from the peak value.

Except for the statistical variance, the mean value of the OFG h_0 can also be extracted from the spectrum, namely, from the peak locations, $h_0 \simeq \Delta_{\rm max}$. This approximation works quite well for small variance, where its deviation, $|(h_0 - \Delta_{\rm max})/h_0|$, is below 10%. As the variance grows, the peak shoulders become broadened, and the peak locations shift to higher frequencies, which deteriorates the resolution.

VI. DISCUSSION AND SUMMARY

We showed an EIT scheme can be established in a quantum dot CQED device by coupling a transmission line to the interdot tunneling gate. The sharp spectral curvature in the EIT window allows for a high-resolution mechanism to extract the statistical information of the nuclear spin bath. According to the order of the OFG strength, different detection strategies are required for an optimal resolution. For singlet-triplet qubit experiments without external polarization of nuclear spins [4,10], the OFG is usually several milliteslas in GaAs quantum dots, much weaker than its charge-noise-induced decay rate of several hundred megahertz. The system is then in the EIT regime where the sharp spectral curvature is available for the detection. When the nuclear spins are polarized with OFG to the order of hundreds of milliteslas [5,13], the system is in the ATS regime, and the bath information is better resolved by the peak structures instead.

The ensemble-averaged result in Eq. (4) is based on the Gaussian distribution of the OFG, where we assumed the two nuclear spin baths are uncorrelated and the statistical variance σ is of the same order as that of a single dot. A partially correlated situation may arise due to, e.g., a strong overlap between the two electron wave functions in each dot or dipolar contributions from spins in the crystal. This would render a narrower statistical variance, in which case our detection scheme becomes more sensitive.

ACKNOWLEDGMENTS

We thank X.-M. Lu and P. Kotetes for helpful discussions. P.-Q.J. acknowledges financial support from the National Natural Science Foundation of China (Grant No. 11304196), as well as the Science and Technology Program

of Shanghai Maritime University. J.J. acknowledges funding from the German Federal Ministry for Research and Education (BMBF) under Grant No. 13XP5063. J.J., A.D.G., and J.H.C. acknowledge the support of the Australian Research Council (Grants No. DP130104381, No. FT160100357, No. DP140100375, No. CE170100026) and the National Computational Infrastructure (NCI), which is supported by the Australian government.

[1] J. Levy, Phys. Rev. Lett. **89**, 147902 (2002).
[2] D. Loss and D. P. DiVincenzo, Phys. Rev. A **57**, 120 (1998).
[3] G. Burkard, D. Loss, and D. P. DiVincenzo, Phys. Rev. B **59**, 2070 (1999).
[4] J. R. Petta, A. C. Johnson, J. M. Taylor, E. A. Laird, A. Yacoby, M. D. Lukin, C. M. Marcus, M. P. Hanson, and A. C. Gossard, Science **309**, 2180 (2005).
[5] S. Foletti, H. Bluhm, D. Mahalu, V. Umansky, and A. Yacoby, Nat. Phys. **5**, 903 (2009).
[6] C. Barthel, D. J. Reilly, C. M. Marcus, M. P. Hanson, and A. C. Gossard, Phys. Rev. Lett. **103**, 160503 (2009).
[7] S. A. Studenikin, J. Thorgrimson, G. C. Aers, A. Kam, P. Zawadzki, Z. R. Wasilewski, A. Bogan, and A. S. Sachrajda, Appl. Phys. Lett. **101**, 233101 (2012).
[8] A. Khaetskii, D. Loss, and L. Glazman, Phys. Rev. B **67**, 195329 (2003).
[9] I. A. Merkulov, Al. L. Efros, and M. Rosen, Phys. Rev. B **65**, 205309 (2002).
[10] W. A. Coish and D. Loss, Phys. Rev. B **72**, 125337 (2005).
[11] W. Yao, R.-B. Liu, and L. J. Sham, Phys. Rev. B **74**, 195301 (2006).
[12] D. Stepanenko, G. Burkard, G. Giedke, and A. Imamoglu, Phys. Rev. Lett. **96**, 136401 (2006).
[13] H. Bluhm, S. Foletti, I. Neder, M. Rudner, D. Mahalu, V. Umansky, and A. Yacoby, Nat. Phys. **7**, 109 (2011).
[14] C. Barthel, J. Medford, C. M. Marcus, M. P. Hanson, and A. C. Gossard, Phys. Rev. Lett. **105**, 266808 (2010).
[15] J. M. Taylor, C. M. Marcus, and M. D. Lukin, Phys. Rev. Lett. **90**, 206803 (2003).
[16] D. J. Reilly, J. M. Taylor, E. A. Laird, J. R. Petta, C. M. Marcus, M. P. Hanson, and A. C. Gossard, Phys. Rev. Lett. **101**, 236803 (2008).
[17] A. Wallraff, D. I. Schuster, A. Blais, L. Frunzio, R.-S. Huang, J. Majer, S. Kumar, S. M. Girvin, and R. J. Schoelkopf, Nature (London) **431**, 162 (2004).
[18] A. Blais, S. M. Girvin, and W. D. Oliver, Nat. Phys. **16**, 247 (2020).
[19] O. Astafiev, K. Inomata, A. O. Niskanen, T. Yamamoto, Yu. A. Pashkin, Y. Nakamura, and J. S. Tsai, Nature (London) **449**, 588 (2007).
[20] S. André, P. Q. Jin, V. Brosco, J. H. Cole, A. Romito, A. Shnirman, and G. Schön, Phys. Rev. A **82**, 053802 (2010).
[21] M. Grajcar, S. H. W. van der Ploeg, A. Izmalkov, E. Ilichev, H.-G. Meyer, A. Fedorov, A. Shnirman, and G. Schön, Nat. Phys. **4**, 612 (2008).
[22] A. A. Houck, D. I. Schuster, J. M. Gambetta, J. A. Schreier, B. R. Johnson, J. M. Chow, J. Majer, L. Frunzio, M. H. Devoret, S. M. Girvin, and R. J. Schoelkopf, Nature (London) **449**, 328 (2007).
[23] B. R. Johnson, M. D. Reed, A. A. Houck, D. I. Schuster, Lev S. Bishop, E. Ginossar, J. M. Gambetta, L. DiCarlo, L. Frunzio, S. M. Girvin, and R. J. Schoelkopf, Nat. Phys. **6**, 663 (2010).
[24] D. Bozyigit, C. Lang, L. Steffen, J. M. Fink, M. Baur, R. Bianchetti, P. J. Leek, S. Filipp, M. P. da Silva, A. Blais, and A. Wallraff, Nat. Phys. **7**, 154 (2011).
[25] M. Fleischhauer, A. Imamoglu, and J. P. Marangos, Rev. Mod. Phys. **77**, 633 (2005).
[26] V. M. Acosta, K. Jensen, C. Santori, D. Budker, and R. G. Beausoleil, Phys. Rev. Lett. **110**, 213605 (2013).
[27] A. I. Lvovsky, B. C. Sanders, and W. Tittel, Nat. Photonics **3**, 706 (2009).
[28] A. D. Greentree, J. H. Cole, A. R. Hamilton, and L. C. L. Hollenberg, Phys. Rev. B **70**, 235317 (2004).
[29] A. A. Abdumalikov, O. Astafiev, A. M. Zagoskin, Y. A. Pashkin, Y. Nakamura, and J. S. Tsai, Phys. Rev. Lett. **104**, 193601 (2010).
[30] J. Joo, J. Bourassa, A. Blais, and B. C. Sanders, Phys. Rev. Lett. **105**, 073601 (2010).
[31] L. Childress, A. S. Sørensen, and M. D. Lukin, Phys. Rev. A **69**, 042302 (2004).
[32] G. Burkard and A. Imamoglu, Phys. Rev. B **74**, 041307(R) (2006).
[33] M. Trif, V. N. Golovach, and D. Loss, Phys. Rev. B **77**, 045434 (2008).
[34] A. Cottet and T. Kontos, Phys. Rev. Lett. **105**, 160502 (2010).
[35] P.-Q. Jin, M. Marthaler, A. Shnirman, and G. Schön, Phys. Rev. Lett. **108**, 190506 (2012).
[36] C. H. Wong and M. G. Vavilov, Phys. Rev. A **95**, 012325 (2017).
[37] T. Frey, P. J. Leek, M. Beck, A. Blais, T. Ihn, K. Ensslin, and A. Wallraff, Phys. Rev. Lett. **108**, 046807 (2012).
[38] K. D. Petersson, L. W. McFaul, M. D. Schroer, M. Jung, J. M. Taylor, A. A. Houck, and J. R. Petta, Nature (London) **490**, 380 (2012).
[39] Y.-Y. Liu, K. D. Petersson, J. Stehlik, J. M. Taylor, and J. R. Petta, Phys. Rev. Lett. **113**, 036801 (2014).
[40] M. J. Gullans, J. Stehlik, Y.-Y. Liu, C. Eichler, J. R. Petta, and J. M. Taylor, Phys. Rev. Lett. **117**, 056801 (2016).
[41] M. J. Gullans, Y.-Y. Liu, J. Stehlik, J. R. Petta, and J. M. Taylor, Phys. Rev. Lett. **114**, 196802 (2015).
[42] M. Mantovani, A. D. Armour, W. Belzig, and G. Rastelli, Phys. Rev. B **99**, 045442 (2019).
[43] B. K. Agarwalla, M. Kulkarni, and D. Segal, Phys. Rev. B **100**, 035412 (2019).
[44] Y.-Y. Liu, J. Stehlik, C. Eichler, X. Mi, T. R. Hartke, M. J. Gullans, J. M. Taylor, and J. R. Petta, Phys. Rev. Lett. **119**, 097702 (2017).
[45] Y.-Y. Liu, T. R. Hartke, J. Stehlik, and J. R. Petta, Phys. Rev. A **96**, 053816 (2017).
[46] J. Lu, R. Wang, J. Ren, M. Kulkarni, and J.-H. Jiang, Phys. Rev. B **99**, 035129 (2019).
[47] T. R. Hartke, Y.-Y. Liu, M. J. Gullans, and J. R. Petta, Phys. Rev. Lett. **120**, 097701 (2018).
[48] C. Müller and T. M. Stace, Phys. Rev. A **95**, 013847 (2017).

[49] C. Karlewski, A. Heimes, and G. Schön, Phys. Rev. B **93**, 045314 (2016).
[50] P.-Q. Jin, M. Marthaler, J. H. Cole, A. Shnirman, and G. Schön, Phys. Rev. B **84**, 035322 (2011).
[51] H. J. Carmichael, *Statistical Methods in Quantum Optics 1* (Springer, Berlin, 2002).
[52] J. Basset, A. Stockklauser, D.-D. Jarausch, T. Frey, C. Reichl, W. Wegscheider, A. Wallraff, K. Ensslin, and T. Ihn, Appl. Phys. Lett. **105**, 063105 (2014).
[53] Z. Ficek and S. Swain, *Quantum Interference and Coherence: Theory and Experiments* (Springer, New York, 2005).
[54] Z. Ficek and S. Swain, Phys. Rev. A **69**, 023401 (2004).
[55] P. M. Anisimov, J. P. Dowling, and B. C. Sanders, Phys. Rev. Lett. **107**, 163604 (2011).
[56] B. Lounis and C. Cohen-Tannoudji, J. Phys. II **2**, 579 (1992).
[57] A. D. Greentree, R. G. Beausoleil, L. C. L. Hollenberg, W. J. Munro, K. Nemoto, S. Prawer, and T. P. Spiller, New J. Phys. **11**, 093005 (2009).